An Iterative Bayesian Compressive Sensing Approach for Reconstructing Non-Born Scatterer

M. Salucci, L. Poli, F. Zardi, L.Tosi, S. Lusa, and A. Massa

2025/04/25

Contents

1 Inhomogeneous Square Object, $\ell = 1.5\lambda$

Test Case Description

Direct solver:

- Side of the investigation domain: $L = 6.0\lambda$
- Cubic domain divided in $\sqrt{D} \times \sqrt{D}$ cells
- Number of cells for the direct solver: $D = 1600$ (discretization $= \lambda/10$)

Investigation domain:

- Cubic domain divided in $\sqrt{N} \times \sqrt{N}$ cells
- Number of cells for the inversion:

  - First Step IMSA: $N^{(1)} = 100$ (discretization $= \lambda/10$)

  - Following Steps IMSA: $N^{(i)}$ not fixed, defined according to the estimated *RoI* $\mathcal{D}^{(i)}$

Measurement domain:

- Total number of measurements: $M = 60$
- Measurement points placed on circles of radius $\rho = 4.5\lambda$

Sources:

- Plane waves
- Number of views: $V = 60$; $\theta_{inc}^{v} = 0 + (v-1) \times (360/V)$
- Amplitude: $A = 1.0$
- Frequency: $F = 300$ MHz ($\lambda = 1$)

Background:

- $\varepsilon_r = 1.0$
- $\sigma = 0$ [S/m]

Scatterer

- Inhomogeneous square object, $\ell = 1.5\lambda$
- $\varepsilon_r^{(1)} \in \{1.20,\ 1.60,\ 2.00\}$ (internal circle)
  $\varepsilon_r^{(2)} = \frac{\varepsilon_r^{(1)}}{2}$ (central circle)
  $\varepsilon_r^{(3)} = \frac{\varepsilon_r^{(1)}}{4}$ (external circle)
- $\sigma = 0$ [S/m]

1.0.1 Inhomogeneous Square Object, $\ell = 1.5\lambda$, $\tau^{(1)} = 0.20$ - (IMSA-BCS) CSI vs. BORN reconstructed profiles

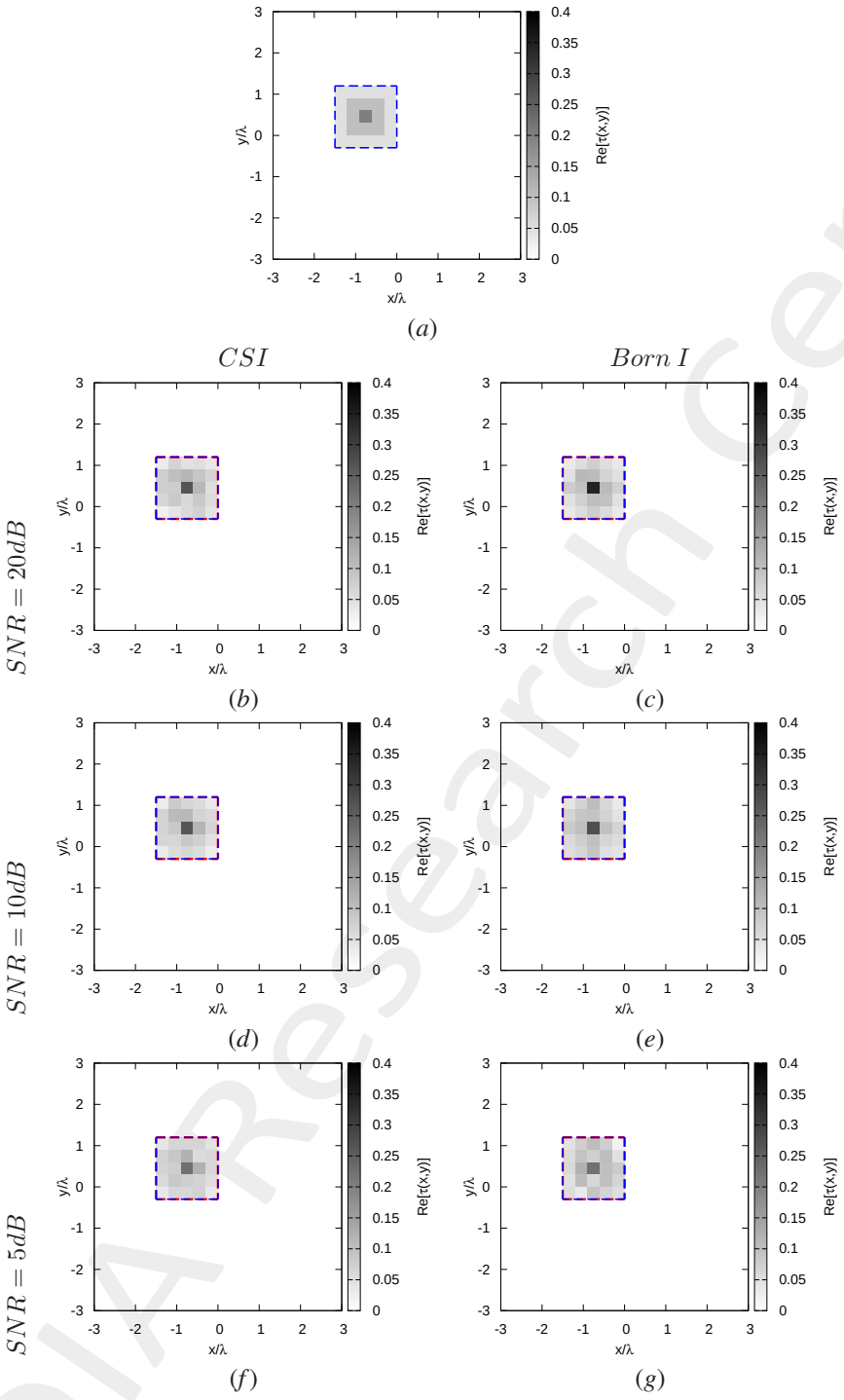

Figure 1: *Inhomogeneous Square Object,* $\ell = 1.5\lambda$, $\tau^{(1)} = 0.20$ - *IMSA-BCS CSI vs. Born I* - (*a*) Actual profile, (*b*)(*d*)(*f*) $IMSA - BCS\ CSI$ and (*c*)(*e*)(*g*) $IMSA - BCS\ Born$ reconstructed profiles for (*b*)(*c*) $SNR = 20$ [dB], (*d*)(*e*) $SNR = 10$ [dB] and (*f*)(*g*) $SNR = 5$ [dB].

	$SNR = 50dB$	
	CSI	$BORN$
ξ_{tot}	1.25×10^{-3}	1.41×10^{-3}
ξ_{int}	1.82×10^{-2}	1.60×10^{-2}
ξ_{ext}	0.00×10^{-1}	0.00×10^{-1}
	$SNR = 20dB$	
	CSI	$BORN$
ξ_{tot}	1.10×10^{-3}	1.38×10^{-3}
ξ_{int}	1.52×10^{-2}	1.57×10^{-2}
ξ_{ext}	0.00×10^{-1}	0.00×10^{-1}
	$SNR = 10dB$	
	CSI	$BORN$
ξ_{tot}	1.14×10^{-3}	1.38×10^{-3}
ξ_{int}	1.68×10^{-2}	1.61×10^{-2}
ξ_{ext}	0.00×10^{-1}	0.00×10^{-1}
	$SNR = 5dB$	
	CSI	$BORN$
ξ_{tot}	1.07×10^{-3}	1.44×10^{-3}
ξ_{int}	1.59×10^{-2}	1.52×10^{-2}
ξ_{ext}	0.00×10^{-1}	0.00×10^{-1}

Table I: *Inhomogeneous Square Object,* $\ell = 1.5\lambda$, $\tau^{(1)} = 0.20$ - ***CSI vs. BORN*** - Reconstrution errors: total (ξ_{tot}), internal (ξ_{int}) and external (ξ_{ext}) errors.

1.0.2 Inhomogeneous Square Object, $\ell = 1.5\lambda$, $\tau^{(1)} = 0.60$ - (IMSA-BCS) CSI vs. BORN reconstructed profiles

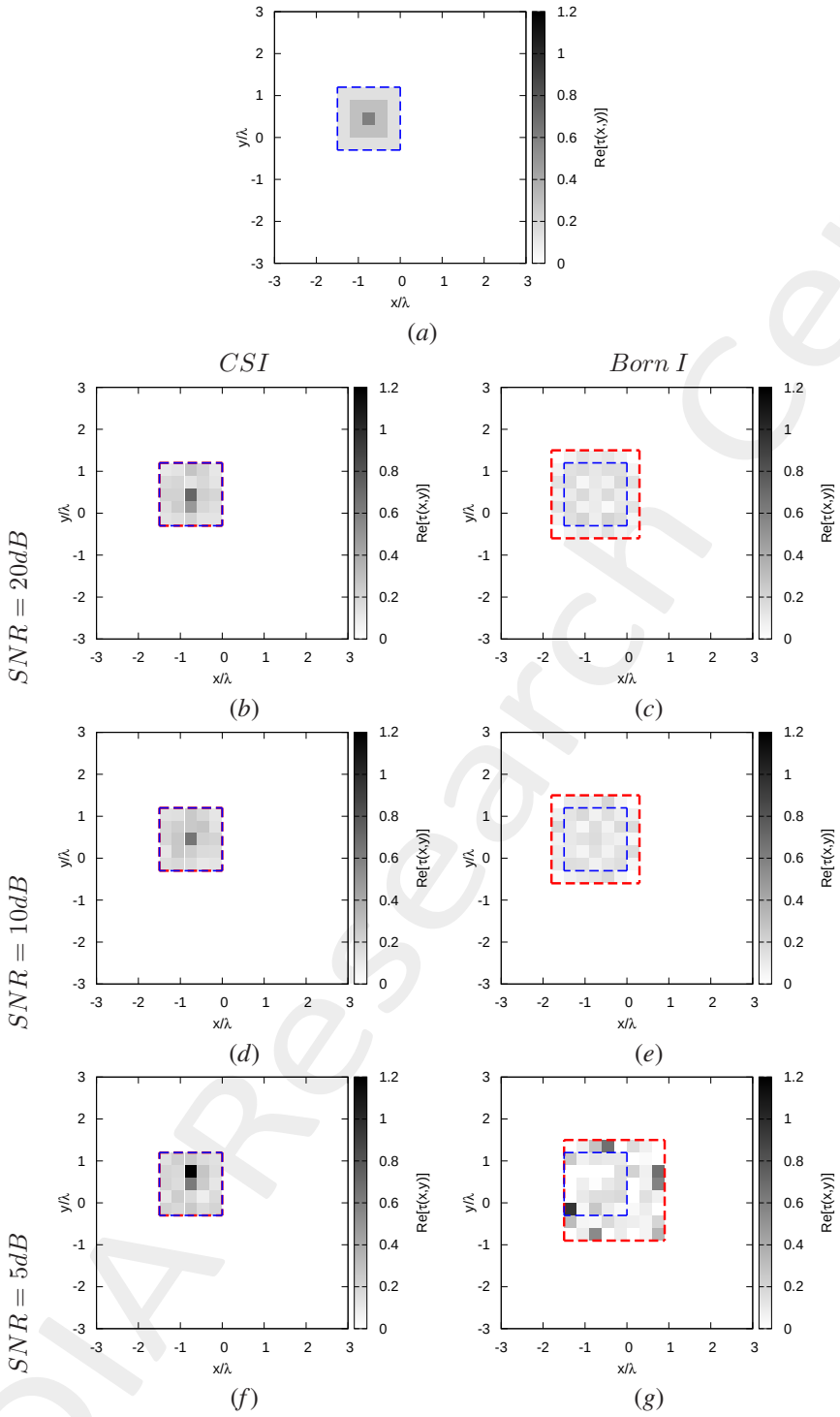

Figure 2: *Inhomogeneous Square Object,* $\ell = 1.5\lambda$, $\tau^{(1)} = 0.60$ - *IMSA-BCS CSI vs. Born I* - (*a*) Actual profile, (*b*)(*d*)(*f*) $IMSA-BCS\ CSI$ and (*c*)(*e*)(*g*) $IMSA-BCS\ Born$ reconstructed profiles for (*b*)(*c*) $SNR = 20$ [dB], (*d*)(*e*) $SNR = 10$ [dB] and (*f*)(*g*) $SNR = 5$ [dB].

	$SNR = 50dB$	
	CSI	$BORN$
ξ_{tot}	3.32×10^{-3}	1.33×10^{-2}
ξ_{int}	4.14×10^{-2}	8.68×10^{-2}
ξ_{ext}	0.00×10^{-1}	5.21×10^{-3}
	$SNR = 20dB$	
	CSI	$BORN$
ξ_{tot}	3.81×10^{-3}	1.24×10^{-2}
ξ_{int}	5.05×10^{-2}	7.95×10^{-2}
ξ_{ext}	0.00×10^{-1}	4.71×10^{-3}
	$SNR = 10dB$	
	CSI	$BORN$
ξ_{tot}	2.77×10^{-3}	1.35×10^{-2}
ξ_{int}	3.40×10^{-2}	8.17×10^{-2}
ξ_{ext}	0.00×10^{-1}	5.62×10^{-3}
	$SNR = 5dB$	
	CSI	$BORN$
ξ_{tot}	1.06×10^{-2}	1.43×10^{-2}
ξ_{int}	1.38×10^{-1}	1.25×10^{-1}
ξ_{ext}	0.00×10^{-1}	2.77×10^{-3}

Table II: *Inhomogeneous Square Object,* $\ell = 1.5\lambda$, $\tau^{(1)} = 0.60$ - ***CSI vs. BORN*** - Reconstrution errors: total (ξ_{tot}), internal (ξ_{int}) and external (ξ_{ext}) errors.

1.0.3 Inhomogeneous Square Object, $\ell = 1.5\lambda$, $\tau^{(1)} = 1.00$ - (IMSA-BCS) CSI vs. BORN reconstructed profiles

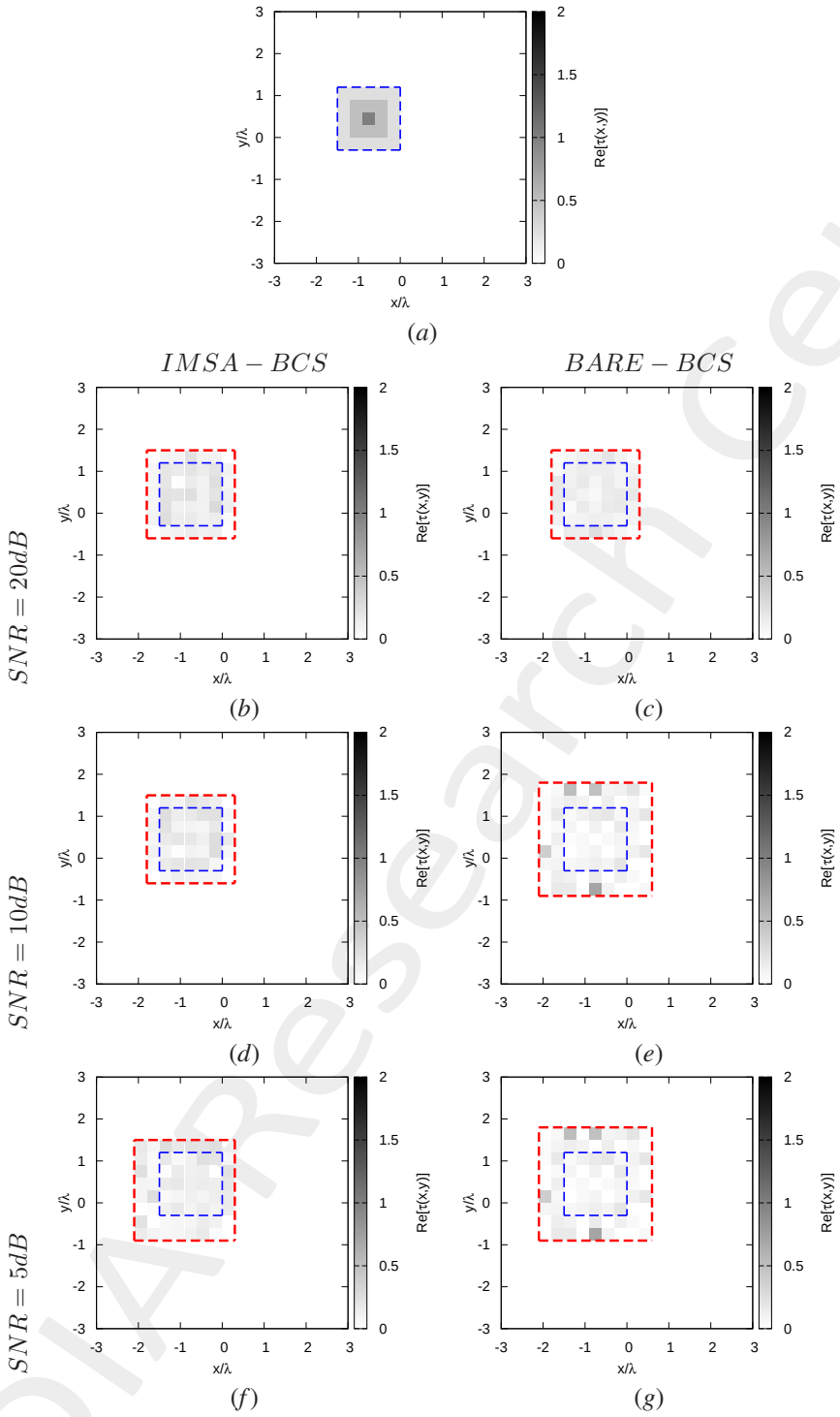

Figure 3: *Inhomogeneous Square Object,* $\ell = 1.5\lambda$, $\tau^{(1)} = 1.00$ - *IMSA-BCS CSI vs. Born I* - (*a*) Actual profile, (*b*)(*d*)(*f*) $IMSA - BCS\ CSI$ and (*c*)(*e*)(*g*) $IMSA - BCS\ Born$ reconstructed profiles for (*b*)(*c*) $SNR = 20$ [dB], (*d*)(*e*) $SNR = 10$ [dB] and (*f*)(*g*) $SNR = 5$ [dB].

	$SNR = 50dB$	
	CSI	$BORN$
ξ_{tot}	1.47×10^{-2}	2.28×10^{-2}
ξ_{int}	1.24×10^{-1}	1.71×10^{-1}
ξ_{ext}	5.63×10^{-3}	8.03×10^{-3}
	$SNR = 20dB$	
	CSI	$BORN$
ξ_{tot}	1.50×10^{-2}	2.18×10^{-2}
ξ_{int}	1.26×10^{-1}	1.65×10^{-1}
ξ_{ext}	5.51×10^{-3}	7.38×10^{-3}
	$SNR = 10dB$	
	CSI	$BORN$
ξ_{tot}	1.55×10^{-2}	3.94×10^{-2}
ξ_{int}	1.33×10^{-1}	1.88×10^{-1}
ξ_{ext}	5.45×10^{-3}	2.08×10^{-2}
	$SNR = 5dB$	
	CSI	$BORN$
ξ_{tot}	2.63×10^{-2}	1.59×10^{-2}
ξ_{int}	1.63×10^{-1}	2.54×10^{-1}
ξ_{ext}	1.39×10^{-2}	0.00×10^{-1}

Table III: *Inhomogeneous Square Object,* $\ell = 1.5\lambda$, $\tau^{(1)} = 1.00$ - ***CSI vs. BORN*** - Reconstrution errors: total (ξ_{tot}), internal (ξ_{int}) and external (ξ_{ext}) errors.

1.1 Punctured Rectangle

Test Case Description

Direct solver:

- Side of the investigation domain: $L = 6.0\lambda$
- Cubic domain divided in $\sqrt{D} \times \sqrt{D}$ cells
- Number of cells for the direct solver: $D = 1600$ (discretization $= \lambda/10$)

Investigation domain:

- Cubic domain divided in $\sqrt{N} \times \sqrt{N}$ cells
- Number of cells for the inversion:

  - First Step IMSA: $N^{(1)} = 100$ (discretization $= \lambda/10$)

  - Following Steps IMSA: $N^{(i)}$ not fixed, defined according to the estimated *RoI* $\mathcal{D}^{(i)}$

Measurement domain:

- Total number of measurements: $M = 60$
- Measurement points placed on circles of radius $\rho = 4.5\lambda$

Sources:

- Plane waves
- Number of views: $V = 60$; $\theta_{inc}^{v} = 0 + (v-1) \times (360/V)$
- Amplitude: $A = 1.0$
- Frequency: $F = 300$ MHz ($\lambda = 1$)

Background:

- $\varepsilon_r = 1.0$
- $\sigma = 0$ [S/m]

Scatterer

- Puntured Rectangle
- $\varepsilon_r \in \{1.05,\ 1.10,\ 1.20,\ 2.00\}$
- $\sigma = 0$ [S/m]

1.1.1 Punctured Rectangle, $\tau = 0.10$ - (IMSA-BCS) CSI vs. BORN reconstructed profiles

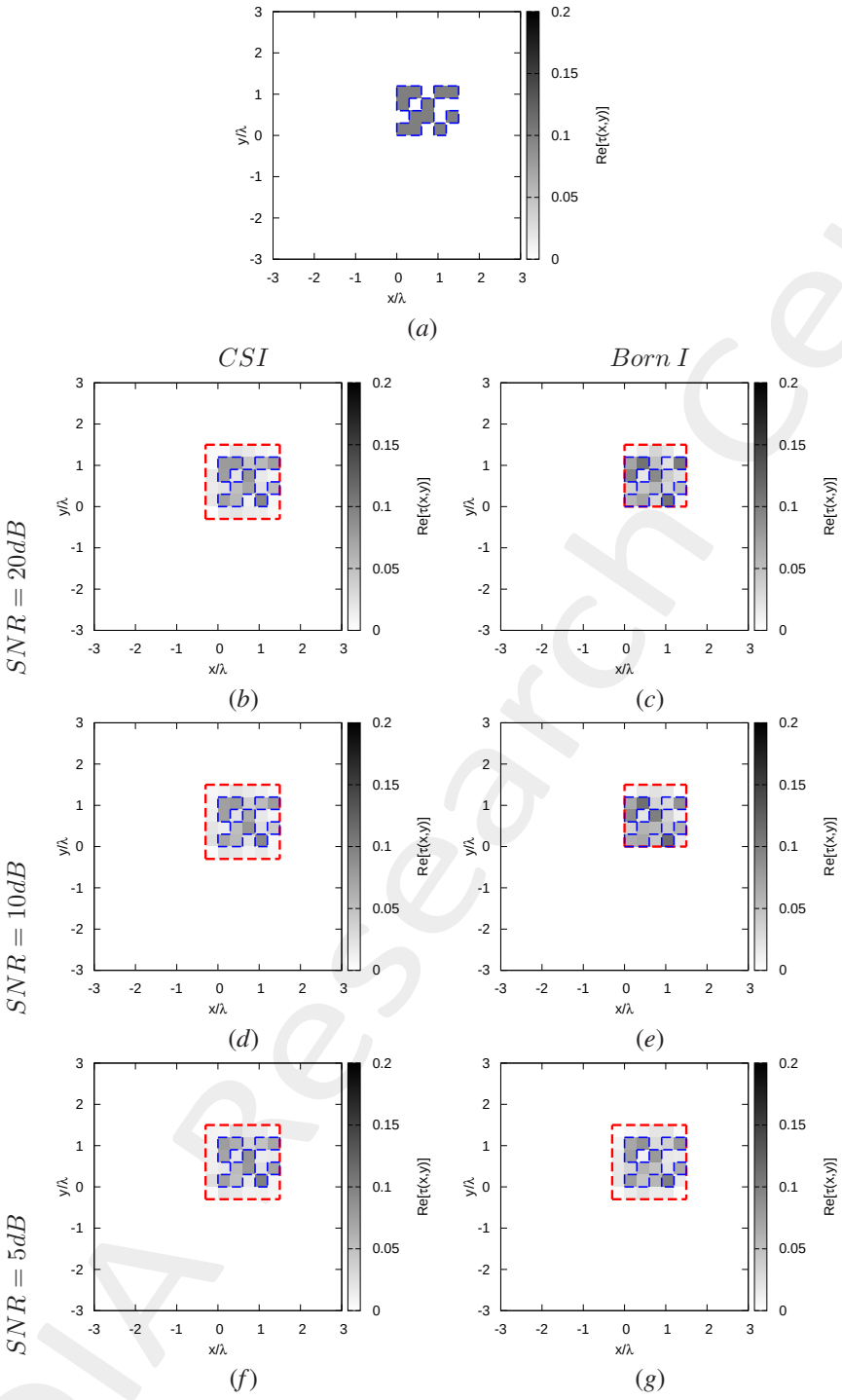

Figure 4: *Punctured Rectangle,* $\tau = 0.10$ - *IMSA-BCS CSI vs. Born I* - (*a*) Actual profile, (*b*)(*d*)(*f*) $IMSA - BCS\ CSI$ and (*c*)(*e*)(*g*) $IMSA - BCS\ Born$ reconstructed profiles for (*b*)(*c*) $SNR = 20$ [dB], (*d*)(*e*) $SNR = 10$ [dB] and (*f*)(*g*) $SNR = 5$ [dB].

	$SNR = 50dB$	
	CSI	$BORN$
ξ_{tot}	1.56×10^{-3}	1.76×10^{-3}
ξ_{int}	2.44×10^{-2}	2.88×10^{-2}
ξ_{ext}	8.09×10^{-4}	8.89×10^{-4}
	$SNR = 20dB$	
	CSI	$BORN$
ξ_{tot}	1.73×10^{-3}	1.64×10^{-3}
ξ_{int}	2.72×10^{-2}	2.71×10^{-2}
ξ_{ext}	9.17×10^{-4}	8.14×10^{-4}
	$SNR = 10dB$	
	CSI	$BORN$
ξ_{tot}	1.84×10^{-3}	1.61×10^{-3}
ξ_{int}	2.88×10^{-2}	2.64×10^{-2}
ξ_{ext}	9.77×10^{-4}	7.89×10^{-4}
	$SNR = 5dB$	
	CSI	$BORN$
ξ_{tot}	1.80×10^{-3}	1.92×10^{-3}
ξ_{int}	2.70×10^{-2}	2.85×10^{-2}
ξ_{ext}	9.71×10^{-4}	1.05×10^{-3}

Table IV: *Punctured Rectangle,* $\tau = 0.10$ - *CSI vs. BORN* - Reconstrution errors: total (ξ_{tot}), internal (ξ_{int}) and external (ξ_{ext}) errors.

1.1.2 Punctured Rectangle, $\tau = 0.20$ - (IMSA-BCS) CSI vs. BORN reconstructed profiles

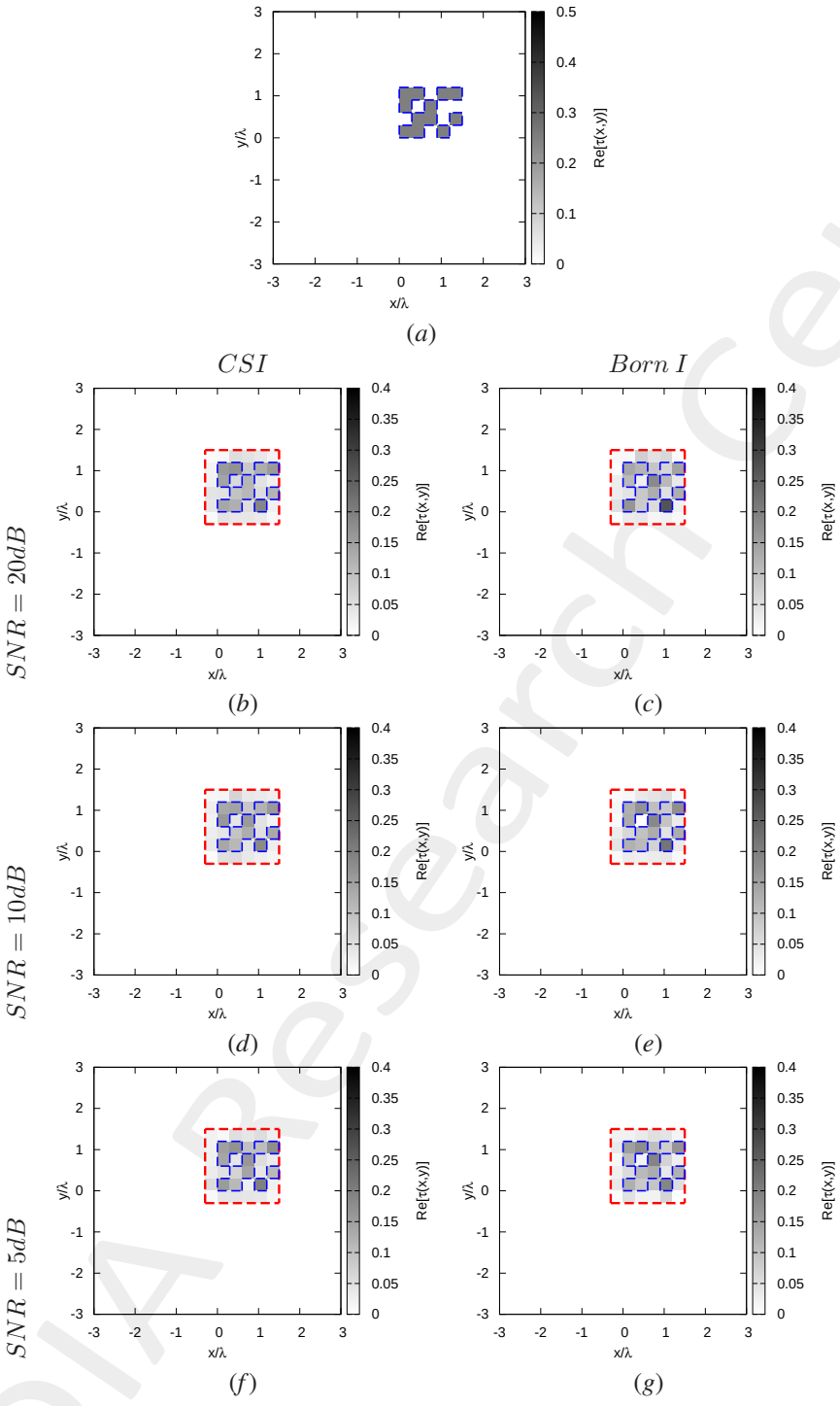

Figure 5: *Punctured Rectangle,* $\tau = 0.20$ - *IMSA-BCS CSI vs. Born I* - (*a*) Actual profile, (*b*)(*d*)(*f*) $IMSA - BCS\ CSI$ and (*c*)(*e*)(*g*) $IMSA - BCS\ Born$ reconstructed profiles for (*b*)(*c*) $SNR = 20$ [dB], (*d*)(*e*) $SNR = 10$ [dB] and (*f*)(*g*) $SNR = 5$ [dB].

	$SNR = 50dB$	
	CSI	$BORN$
ξ_{tot}	3.81×10^{-3}	4.68×10^{-3}
ξ_{int}	5.15×10^{-2}	6.63×10^{-2}
ξ_{ext}	2.25×10^{-3}	2.40×10^{-3}
	$SNR = 20dB$	
	CSI	$BORN$
ξ_{tot}	3.83×10^{-3}	4.50×10^{-3}
ξ_{int}	5.19×10^{-2}	6.41×10^{-2}
ξ_{ext}	2.21×10^{-3}	2.28×10^{-3}
	$SNR = 10dB$	
	CSI	$BORN$
ξ_{tot}	3.73×10^{-3}	4.09×10^{-3}
ξ_{int}	5.08×10^{-2}	5.29×10^{-2}
ξ_{ext}	2.18×10^{-3}	2.17×10^{-3}
	$SNR = 5dB$	
	CSI	$BORN$
ξ_{tot}	3.81×10^{-3}	4.34×10^{-3}
ξ_{int}	4.94×10^{-2}	5.36×10^{-2}
ξ_{ext}	2.25×10^{-3}	2.33×10^{-3}

Table V: *Punctured Rectangle,* $\tau = 0.20$ - *CSI vs. BORN* - Reconstrution errors: total (ξ_{tot}), internal (ξ_{int}) and external (ξ_{ext}) errors.

	$SNR = 50dB$	
	CSI	$BORN$
ξ_{tot}	1.84×10^{-2}	2.64×10^{-2}
ξ_{int}	3.12×10^{-1}	4.36×10^{-1}
ξ_{ext}	7.56×10^{-3}	5.84×10^{-3}
	$SNR = 20dB$	
	CSI	$BORN$
ξ_{tot}	2.19×10^{-2}	2.63×10^{-2}
ξ_{int}	3.18×10^{-1}	4.33×10^{-1}
ξ_{ext}	1.00×10^{-2}	5.72×10^{-3}
	$SNR = 10dB$	
	CSI	$BORN$
ξ_{tot}	2.37×10^{-2}	2.75×10^{-2}
ξ_{int}	5.00×10^{-1}	4.40×10^{-1}
ξ_{ext}	8.55×10^{-3}	6.24×10^{-3}
	$SNR = 5dB$	
	CSI	$BORN$
ξ_{tot}	4.83×10^{-2}	3.14×10^{-2}
ξ_{int}	4.18×10^{-1}	4.44×10^{-1}
ξ_{ext}	3.03×10^{-2}	9.02×10^{-3}

Table VI: *Punctured Rectangle,* $\tau = 1.00$ - *CSI vs. BORN* - Reconstrution errors: total (ξ_{tot}), internal (ξ_{int}) and external (ξ_{ext}) errors.

1.1.3 Punctured Rectangle - (IMSA-BCS) CSI vs. BORN errors resume vs. τ

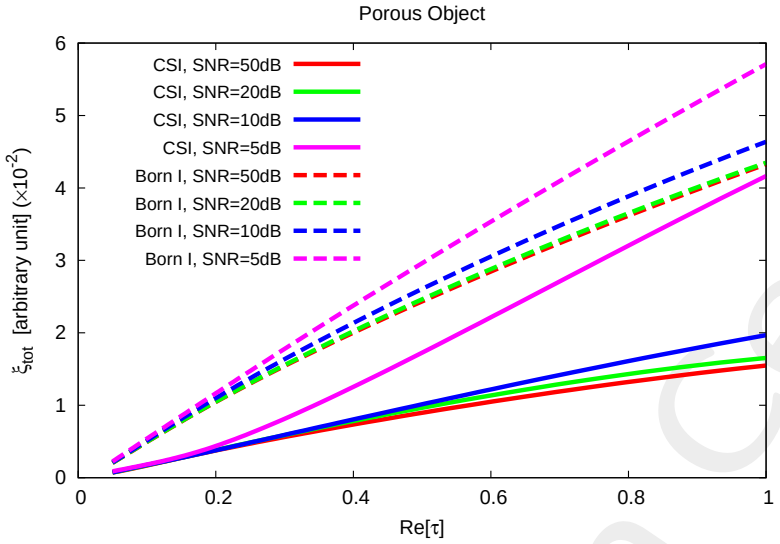

(*a*)

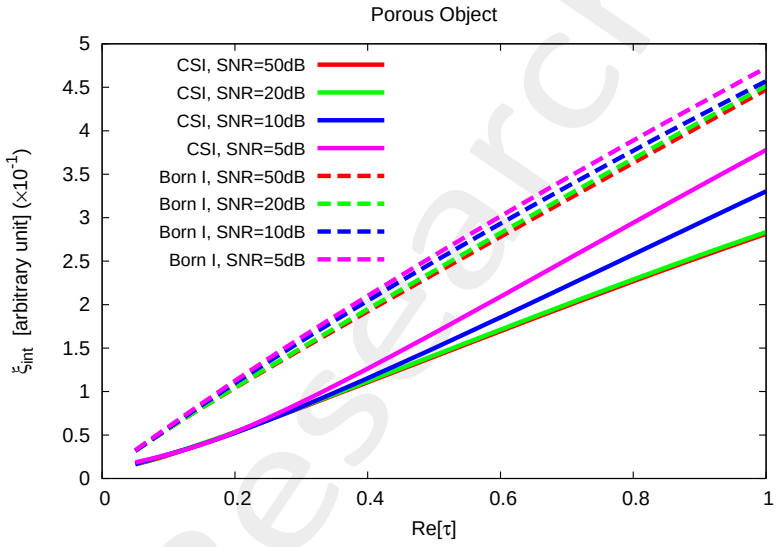

(*b*)

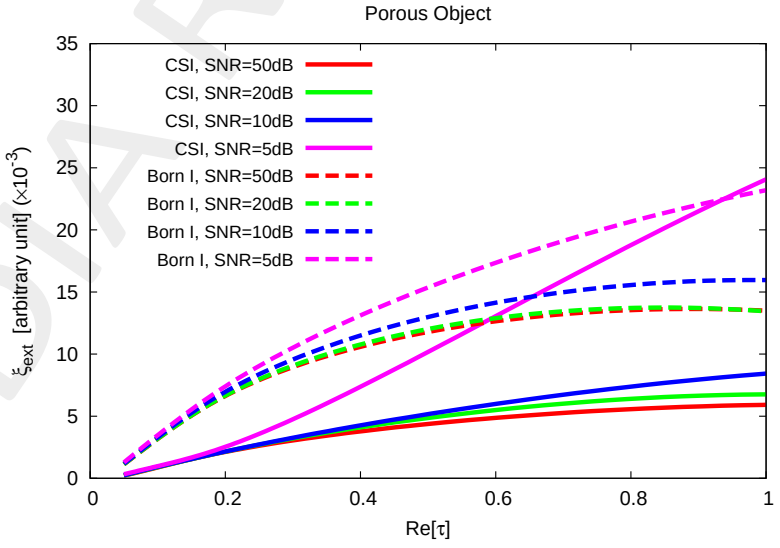

(*c*)

Figure 6: *Punctured Rectangle* - Reconstruction errors vs. τ: (*a*) total error, (*b*) internal error and (*c*) external error.

More information on the topics of this document can be found in the following list of references.

References

[1] G. Oliveri, M. Salucci, N. Anselmi, and A. Massa, "Compressive sensing as applied to inverse problems for imaging: theory, applications, current trends, and open challenges," *IEEE Antennas Propag. Mag. - Special Issue on 'Electromagnetic Inverse Problems for Sensing and Imaging,'* vol. 59, no. 5, pp. 34-46, Oct. 2017 (DOI: 10.1109/MAP.2017.2731204).

[2] A. Massa, P. Rocca, and G. Oliveri, "Compressive sensing in electromagnetics - A review," *IEEE Antennas Propag. Mag*., pp. 224-238, vol. 57, no. 1, Feb. 2015 (DOI: 10.1109/MAP.2015.2397092).

[3] A. Massa and F. Texeira, "Guest-Editorial: Special Cluster on Compressive Sensing as Applied to Electromagnetics," *IEEE Antennas Wirel. Propag. Lett.*, vol. 14, pp. 1022-1026, 2015 (DOI: 10.1109/LAWP.2015.2425011).

[4] M. Salucci, L. Poli, F. Zardi, L. Tosi, S. Lusa, and A. Massa, "Contrast source inversion of sparse targets through multi-resolution Bayesian compressive sensing," *Inverse Probl.*, vol. 40, no. 5, p. 055016, May 2024 (DOI 10.1088/1361-6420/ad3b33).

[5] G. Oliveri, N. Anselmi, M. Salucci, L. Poli, and A. Massa, "Compressive sampling-based scattering data acquisition in microwave imaging," *J. Electromagn. Waves Appl.* J, vol. 37, no. 5, 693-729, Mar. 2023 (DOI: 10.1080/09205071.2023.2188263).

[6] G. Oliveri, L. Poli, N. Anselmi, M. Salucci, and A. Massa, "Compressive sensing-based Born iterative method for tomographic imaging," *IEEE Tran. Microw. Theory Techn.*, vol. 67, no. 5, pp. 1753-1765, May 2019 (DOI: 10.1109/TMTT.2019.2899848).

[7] M. Salucci, L. Poli, and G. Oliveri, "Full-vectorial 3D microwave imaging of sparse scatterers through a multi-task Bayesian compressive sensing approach," *Journal of Imaging*, vol. 5, no. 1, pp. 1-24, Jan. 2019 (DOI: 10.3390/jimaging5010019).

[8] M. Salucci, A. Gelmini, L. Poli, G. Oliveri, and A. Massa, "Progressive compressive sensing for exploiting frequency-diversity in GPR imaging," *J. Electromagn. Waves Appl. J*, vol. 32, no. 9, pp. 1164-1193, 2018 (DOI: 10.1080/09205071.2018.1425160).

[9] N. Anselmi, L. Poli, G. Oliveri, and A. Massa, "Iterative multi-resolution bayesian CS for microwave imaging," *IEEE Trans. Antennas Propag.*, vol. 66, no. 7, pp. 3665-3677, Jul. 2018 (DOI: 10.1109/TAP.2018.2826574).

[10] N. Anselmi, G. Oliveri, M. A. Hannan, M. Salucci, and A. Massa, "Color compressive sensing imaging of arbitrary-shaped scatterers," *IEEE Trans. Microw. Theory Techn.*, vol. 65, no. 6, pp. 1986-1999, Jun. 2017 (DOI: 10.1109/TMTT.2016.2645570).

[11] N. Anselmi, G. Oliveri, M. Salucci, and A. Massa, "Wavelet-based compressive imaging of sparse targets," *IEEE Trans. Antennas Propag.*, vol. 63, no. 11, pp. 4889-4900, Nov. 2015 (DOI: 10.1109/TAP.2015.2444423).

[12] G. Oliveri, P.-P. Ding, and L. Poli, "3D crack detection in anisotropic layered media through a sparseness-regularized solver," *IEEE Antennas Wirel. Propag. Lett.*, vol. 14, pp. 1031-1034, 2015 (DOI: 10.1109/LAWP.2014.2365523).

[13] L. Poli, G. Oliveri, P.-P. Ding, T. Moriyama, and A. Massa, "Multifrequency Bayesian compressive sensing methods for microwave imaging," *J. Opt. Soc. Am. A*, vol. 31, no. 11, pp. 2415-2428, 2014 (DOI: 10.1364/JOSAA.31.002415).

[14] G. Oliveri, N. Anselmi, and A. Massa, "Compressive sensing imaging of non-sparse 2D scatterers by a total-variation approach within the Born approximation," *IEEE Trans. Antennas Propag.*, vol. 62, no. 10, pp. 5157-5170, Oct. 2014 (DOI: 10.1109/TAP.2014.2344673).